Optical characterization of two cataclysmic variables: RBS 0490 and SDSS J075939.79+191417.3

Arti Joshi, ¹ J.C.Pandey, ² Nikita Rawat, ² Ashish Raj, ³ Wei Wang, ^{1,4,*} and H. P. Singh³

School of Physics and Technology, Wuhan University, Wuhan 430072, China
Aryabhatta Research Institute of Observational Sciences (ARIES), Nainital - 263002, India
Department of Physics and Astrophysics, University of Delhi, 110007 Delhi, India
WHU-NAOC Joint Center for Astronomy, Wuhan University, Wuhan 430072, China

ABSTRACT

We present optical photometric and spectroscopic observations of two Cataclysmic Variables (CVs), namely RBS 0490 and SDSS J075939.79+191417.3. The optical variations of RBS 0490 have been found to occur at the period of 1.689 ± 0.001 hr which appears to be a probable orbital period of the system. Present photometric observations of SDSS J075939.79+191417.3 confirm and refine the previously determined orbital period as 3.14240928 ± 0.00000096 hr. The presence of long-duration eclipse features in the light curves of SDSS J075939.79+191417.3 indicates eclipses might be due to an accretion disc and bright spot. The orbital inclination of SDSS J075939.79+191417.3 is estimated to be $\sim 78^\circ$ using the eclipse morphology. The phased-light curve variations during the orbital cycle of RBS 0490 provide evidence of the emission from an independent second accretion region or a second fainter pole. Optical spectra of RBS 0490 and SDSS J075939.79+191417.3 show the presence of strong Balmer, weak He II (λ 4686) emission lines, along with the detection of strong $H\beta$ emission lines with a large value of equivalent width. The characteristic features of RBS 0490 seem to favour low-field polars, while SDSS J075939.79+191417.3 appears to be similar to the non-magnetic systems.

Keywords: Cataclysmic Variable stars(203), Semi-detached binary stars(1443), Magnetic fields(994), eclipsing — stars: individual: RBS 0490 — stars: individual: SDSS J075939.79+191417.3

1. INTRODUCTION

Cataclysmic Variables are semi-detached close binary systems in which white dwarf (WD) primary accretes material from the mass donating secondary via Roche-lobe overflow (Warner 1995). The material transferred from the secondary flows through the inner Lagrangian point and orbits around the primary, forming an accretion disc in non-magnetic systems. However, if the magnetic field strength of the WD is large enough, an accretion disc can form far from the WD, but the inner disc disrupts at the magnetospheric radius, and the field forces material to fall onto the poles of the WD. In these systems, $P_{\omega} < P_{\Omega}$, where P_{ω} and P_{Ω} are spin and orbital periods, respectively, and are known as Intermediate Polars (IPs) (Patterson 1994, and references therein). Alternately, if the magnetic field of the WD is sufficiently strong, the magnetic pressure exceeds the ram pressure, preventing the formation of an accretion disc. The accreted matter follows the magnetic field lines of the WD and dumps onto the poles (see Cropper 1990; Warner 1995). These binary systems are known as polars for which $P_{\omega} = P_{\Omega}$. The majority of polars have orbital periods shorter than the 'period gap of 2-3 hr' (Scaringi et al. 2010). The optical and near-infrared radiations in these systems are dominated by cyclotron emission and originate from the accretion column near the WD in the post-shock region. These systems tend to show periodic modulation at the orbital period, and their optical spectra exhibit strong Balmer emission lines along with He I and He II emission lines (Warner 1986, and references therein). The H β and HeII (λ 4686 Å) emission lines are much stronger in polars and usually originate in the accretion column. The majority of the polars are single-pole accretors (e.g. Schwope et al. 1993; Salvi et al. 2002; Bridge et al. 2003), whereas some polars accrete onto both poles (e.g. Beardmore et al. 1995; Schwope et al. 1995; Schmidt et al. 1999) and some other switch between single and double pole accretion (e.g., Rosen et al. 1996; Mason et al. 1998). In this paper, we present detailed analyses of two CVs namely RBS 0490 and SDSS J075939.79+191417.3 (hereafter J0759) using the optical photometric and spectroscopic observations that were taken between the years 2005 and 2021.

RBS 0490 was detected during the *ROSAT* all-sky survey (RASS; Voges et al. 1999; Schwope et al. 2002) and found to be *ROSAT* bright source. Inverting the Gaia parallax of RBS 0490 gives a distance of 320±11 pc (Gaia Collaboration et al.

^{*} Corresponding author wangwei2017@whu.edu.cn

Table 1. Log of optical photometric and spectroscopic observations of RBS 0490 and J0759.

Object	Date of	Facility	Instrument	Filter/	Integration	Time	Time-span
	Observations			Band	Time (s)	$(\mathbf{J}\mathbf{D}_t)$	(hr)
RBS 0490	2015 Oct 10	1.04 m - ST	1k×1k CCD	R	300	2457305.00	3.52
	2015 Nov 06	1.3 m - DFOT	512×512 CCD	R	200	2457333.00	3.87
	2017 Dec 22	2.01 m - HCT	HFOSC/Gr7	380-780 nm	3600	2458110.08	1.00
	2018 Nov 30	2.01 m - HCT	HFOSC/Gr7	380-780 nm	3000	2458453.27	0.83
J0759	2016 Mar 07	1.3 m - DFOT	512×512 CCD	R	300	2457455.00	4.11
	2021 Feb 06	1.3 m - DFOT	2k×2k CCD	R	300	2459252.00	3.49
	2021 Feb 07	1.3 m - DFOT	2k×2k CCD	R	300	2459253.00	3.40
	2021 Feb 08	1.3 m - DFOT	2k×2k CCD	R	300	2459254.00	3.52
	2021 Feb 15	1.04 m - ST	4k×4k CCD	R	300	2459261.00	3.24
	2018 Dec 17	2.01 m - HCT	HFOSC/Gr7	380-780 nm	3600	2458470.39	1.00
	2019 Feb 09	2.01 m - HCT	HFOSC/Gr7	380-780 nm	3600	2458524.36	1.00
	2020 Jan 14	2.01 m - HCT	HFOSC/Gr7	380-780 nm	2700	2458863.45	0.75
	2021 Mar 31	2.01 m - HCT	HFOSC/Gr7	380-780 nm	3600	2459305.08	1.00
	2021 Apr 24	2.01 m - HCT	HFOSC/Gr7	380-780 nm	3600	2459329.10	1.00

Note—JD_t for HFOSC is the start time of the observations, whereas for photometric observation it is observation day.

2021). Schwope et al. (2002) constructed a spectrum from 87 photons detected in the RASS and suggested that it can be modeled with a thermal bremsstrahlung component at a temperature of 20 keV. All emission lines appeared double-peaked in the optical spectrum of Schwope et al. Moreover, H-Balmer and He I emission lines (2002).were very prominent, whereas He II emission lines were relatively weak. Later, Thorstensen et al. (2006) found a candidate 46-min radial-velocity period. In contrast to Schwope et al. (2002), Thorstensen et al. (2006) found single-peaked emission lines, and only moderately strong He II $\lambda 4686$. Harrison & Campbell (2015) have analysed the infrared data obtained from the Wide-field Infrared Survey Explorer (WISE) bands and suggested that it is a polar.

J0759 was identified as a CV by Szkody et al. (2006) based on the optical spectrum obtained during the Sloan Digital Sky Survey (SDSS). The SDSS spectrum shows strong Balmer emission (H β has an equivalent width (EW) of 72 Å), and a He II(λ 4686)/H β EW ratio of 0.2. Subsequently, they reported that J0759 reveals the strength of He II (λ 4686 Å) larger than most dwarf novae but not quite up to the values typical for polars or IPs. Later, Gänsicke & Dillon (2009) reported the orbital period of ~ 188.45 min for J0759 using

the SDSS spectroscopy. However, a much refined period of 0.1309337 d is reported in the AAVSO VSX catalog based on the data obtained from the Catalina Real-time Transit Survey (CRTS) and Zwicky Transient Facility (ZTF). Using the Gaia parallax (Gaia Collaboration et al. 2021), the distance of J0759 is calculated to be 1873±535 pc.

The paper is organized as follows. We summarize the description of observations and data reduction in the next section. Analyses and the results of the optical data are described in section 3. Finally, we present discussion and conclusions in sections 4 and 5, respectively.

2. OBSERVATIONS AND DATA REDUCTION

2.1. Optical Photometric Observations

R-band photometric observations of both sources were carried out during epochs 2015, 2016, and 2021 using the 1.04-m Sampuranand Telescope (ST; Sinvhal et al. 1972) and 1.3-m Devasthal Fast Optical Telescope (DFOT; Sagar et al. 2011) of ARIES, Nainital, India. A detailed log for photometric observations is given in Table 1. The ST was equipped with a 1k×1k CCD and 4k×4k CCD during observations of epochs 2015 and 2021, respectively. However, the DFOT was equipped with CCDs 2k×2k during the epoch 2021 and 512

Table 2. Comparison stars used for the differential photometry for RBS 0490 and J0759.

Object	Reference	B1	R1	B2	R2
	USNO-B1.0	(mag)	(mag)	(mag)	(mag)
RBS 0490	0731-0063800	16.89	16.53	18.30	17.11
'C1'	0731-0063769	15.20	13.96	15.26	14.12
'C2'	0731-0062447	16.63	14.66	16.95	15.40
J0759	1092-0155844	18.26	18.50	18.65	17.84
'C1'	1092-0155866	16.81	15.78	16.79	15.63
'C2'	1092-0155859	17.13	15.73	16.94	15.65

Note—C1 and C2 stands for comparison 1 and 2 for each program star.

× 512 during observations of epochs 2015 and 2016. Several bias and twilight sky flat frames were also acquired during each observing run. Pre-processing of each observed frame was performed using IRAF¹ software. To obtain the instrumental magnitudes, the differential photometry in a manner variable minus comparison star was performed by using a comparison star in the same field. The details of the adopted comparison stars labeled as 'C1' and 'C2' for each source are given in Table 2. The constant brightness of comparison stars was checked by inspecting the light curves of 'C1-C2' for each source separately. For consecutive epoch of observations (see Table 1), the nightly mean of the standard deviation of 'C1-C2' were derived as 0.0052 and 0.0045 for RBS 0490, and 0.0055, 0.0024, 0.0040, 0.0040, and 0.0091 for J0759. Finally, the R-band magnitudes of observations were computed with respect to comparison star 'C1'.

2.2. TESS, ZTF, and CRTS Observations

RBS 0490 was observed by the Transiting Exoplanet Survey Satellite (TESS) with camera 2 in sector 31 for 25 days at a two-minute cadence from 22 October 2020 to 16 November 2020. TESS was launched on 18 April 2019 into a 13.7 d orbit. It has four small telescopes with four cameras with field of view of each 24×24 degree² are aligned to cover 24 × 90-degree strips of the sky called 'sectors' (see Ricker et al. 2015, for details). TESS bandpass extends from 600 to 1000 nm with an effective wavelength of 800 nm. TESS observations of RBS 0490 were continuous except for ~ 56.8-hour gap halfway into the sector. The data of RBS 0490 was stored under Mikulski Archive for Space Telescopes (MAST) data archive with identification number 'TIC 279483438'. Data taken during an anomalous event had quality flags greater

than 0 in the FITS file data structure and thus we have considered only the data with the 'QUALITY flag' = 0. We have taken PDCSAP flux values, which is the Simple Aperture Photometry flux after they have been corrected for systematic trends common to all-stars.

The ZTF is a northern-sky synoptic optical survey for high cadence time-domain astronomy, which used the Palomar 48-inch (P48) telescope (Graham et al. 2019; Bellm et al. 2019; Dekany et al. 2020). Its CCD camera consists of 16 6K×6K E2V CCDs, producing a 47 deg² field of view. There are three available filters, ZTF-g, ZTF-r, and ZTF-i. Exposure times are usually 30 seconds for g and r bands and 60 seconds for i band. RBS 0490 and J0759 were observed by ZTF between 2018 to 2021. ZTF lists a total of 339 exposures for RBS 0490 from 23 September 2018 to 26 February 2021 and 520 exposures for J0759 from 28 March 2018 to 24 April 2021.

J0759 was also observed by the CRTS (Drake et al. 2009, 2014) between 09 April 2005 to 24 December 2013 in the V-filter. CRTS combines three distinct surveys—the Mount Lemmon Survey (MLS) and the Catalina Schmidt Survey (CSS) in the Northern Hemisphere and the Siding Spring Survey (SSS) in the South. The CRTS data of J0759 is available from the MLS and CSS surveys, and its light curves are easily accessible online.

2.3. Optical Spectroscopic Observations

We obtained long-slit low-resolution optical spectra of both sources between the year 2017 to 2021 using the 2.01m Himalayan Chandra Telescope at IAO, Hanle which is equipped with the Hanle Faint Object Spectrograph and Camera (HFOSC; Prabhu & Anupama 2010). A detailed log of the spectroscopic observations is given in Table 1. For all epochs, the observations were taken using the grism Gr7 (3800-7800) Å with a resolution of 1330 and dispersion of 1.45 Å/pixel. Spectrophotometric standard stars were also observed during each observing run. The data reduction of the standard and program stars was accomplished with the three main steps using IRAF tasks: pre-processing, wavelength calibration, and flux calibration. Lamp spectra of Fe-Ar were used for the wavelength calibration. The night sky emission lines 5577 Å, 6300 Å, and 6363 Å were used to check the appropriate shift, and the shift was then applied with SPECSHIFT task wherever it was required.

3. ANALYSIS AND RESULTS

3.1. RBS 0490

3.1.1. Light Curve Morphology and Power Spectra

Figure 1(a) combines the TESS, ZTF-r/g, and our own R-band observations of RBS 0490 from the year 2015 to 2021. To probe RBS 0490 in more detail, we have closely inspected its light curve observed from each facility independently. The full TESS light curve of RBS 0490 and zoomed version of

¹ IRAF is distributed by the national optical astronomy observatories, USA.

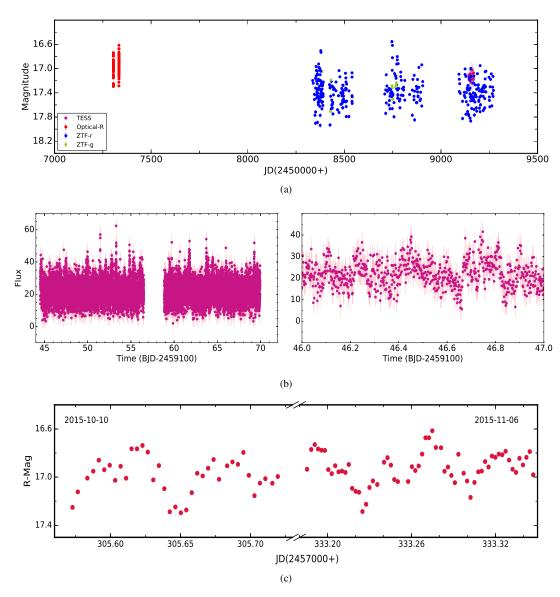


Figure 1. (a) Combined R-band, TESS, and ZTF-r/g light curves of RBS 0490, (b) the full TESS light curve of RBS 0490, where the right panel shows zoomed version of the one-day observation, and (c) R-band light curves of RBS 0490 for two epochs of observations.

its one-day observations are shown in Figure 1(b), whereas the R-band light curves are shown in Figure 1(c). Its light curve variations are associated mostly with the bright maxima along with minima and exhibit a periodic nature of the system. The periodic nature of the system has been demonstrated by applying the Lomb-Scargle (LS) periodogram algorithm (Lomb 1976; Scargle 1982; Horne & Baliunas 1986) to the entire TESS, ZTF-r, and R-band observations. The LS power spectrum of the TESS data of RBS 0490 is shown in the top panel of Figure 2. The observed highest significant peak in the TESS power spectrum corresponds to the period of 1.689±0.001 hr which is found to lie above the 99% confidence level. The significance of this detected peak is determined by calculating the False Alarm Probability (FAP; Horne & Baliunas 1986). The confidence level is represented

by the dotted red lines. In contrast to radial-velocity measurements of Thorstensen et al. (2006), we have not detected any significant period near 46 min. We provisionally identify the 1.689-hr period with P_{Ω} .

From the R-band photometric data, we have detected a significant period of $1.689\pm0.001\,\mathrm{hr}$ which is exactly similar to the period derived from the TESS data. The LS power spectrum obtained from the photometric data is shown in the middle panel of Figure 2. The ZTF-r band light curve of RBS 0490 is very sparse and resulted in a noisy power spectrum as shown in the bottom panel of Figure 2. The orbital frequency obtained from the ZTF data is also marked in this figure. The significant periods derived from the LS photometric, TESS, and ZTF data are given in Table 3.

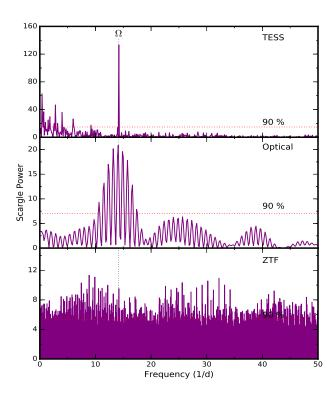


Figure 2. The Lomb-Scargle power spectra of RBS 0490 obtained from the complete data set of the TESS, R-band, and ZTF-r band observations. The horizontal dotted lines in the Lomb-Scargle power spectra represent the 90 % confidence level.

Table 3. Periods corresponding to dominant peaks in the power spectra of RBS 0490 and J0759 obtained from the R-band photometry, TESS, ZTF, and CRTS observations.

Period(hr)	R-BAND PHOTOMETRY	TESS/CRTS*	ZTF
		RBS 0490	
P_{Ω}	1.6894 ± 0.0011	1.6894 ± 0.0012	1.6895 ± 0.0003
		J0759	
P_{Ω}	3.149025 ± 0.011338	3.142396 ± 0.000032	3.142387 ± 0.000092
$P_{2\Omega}$	1.573160 ± 0.002824	1.571206±0.000008	1.571194±0.000023
$P_{3\Omega}$	1.054452 ± 0.001268	1.047469 ± 0.000004	1.047473 ± 0.000010
$P_{4\Omega}$	0.789414 ± 0.000711	0.789678 ± 0.000002	0.785603 ± 0.000006

^{*}Period obtained from TESS data for RBS 0490 and CRTS data for J0759.

3.1.2. Orbital-Phased Light Curve Variations and System's Geometry

We explored the phased-light curve variation of RBS 0490 during its binary motion. Light curves obtained from the TESS and R-band observations are folded using the time of first observation JD=2457305.572836 as the reference epoch. However, the sparse light curve spanning over several years in the ZTF-r band is not useful to produce meaningful phase-dependent light curve variations. Phase-folded light curves with phase bins of 0.0222 and 0.05 for TESS and R-band

observations, respectively are shown in Figure 3. Though, the R-band light curve is less extensive yet both TESS and R-band light curves appear to show almost consistent light curve variation. However, a careful inspection of the phased light curve from the TESS observations shows double-humped-like features which are separated by an orbital phase of 0.5, whereas the phased R-band light curve shows a plateau-like structure followed by a broad hump.

Using the mean empirical mass-period relation given by Smith & Dhillon (1998), we have derived the mass and radius

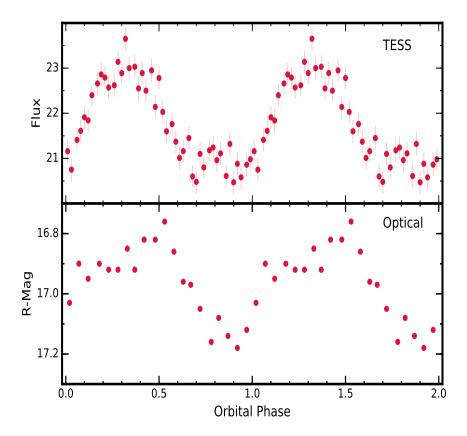


Figure 3. Orbital-phase-folded light curves of RBS 0490 obtained from the TESS and R-band observations with phase bin of 0.0222 and 0.05, respectively.

of the secondary as $0.10(\pm0.02)~M_{\odot}$ and $0.16(\pm0.01~R_{\odot})$, respectively. Using an orbital period of 1.689 hr, we have estimated the mean density of secondary, $\overline{\rho}$ =36.8 g cm⁻³ (see Warner 1995, for formulae), which corresponds to a lower main-sequence star of spectral class M5.6 and an effective temperature of 2975 K (see Beuermann et al. 1998; Knigge 2006). Using the mass range of WD of 0.2–1.5 M_{\odot} in CVs (Zorotovic et al. 2011), the binary separation (a) is estimated to be in the range of (3.3–5.8)×10¹⁰ cm.

3.1.3. Optical Spectroscopy

Optical spectra with a wealth of spectral features was observed for RBS 0490 during two different epochs of observations. Figure 4 shows the optical spectra of RBS 0490 for epochs 22 December 2017 and 30 November 2018. Identification, flux, EW, and FWHM of the principal emission lines of RBS 0490 obtained through a single-Gaussian fitting are given in Table 4. Optical spectra of RBS 0490 exhibit a flat continuum and strong Balmer emission lines (from $H\alpha$ - $H\zeta$), He I, and He II emission lines. The HeII λ 4686 line is only modestly strong. The observed spectra resemble the spectra of Schwope et al. (2002) and Thorstensen et al. (2006) observed during epochs 1997, 1998, and 2002. Similar to Thorstensen et al. (2006), we observed all the spectral lines as single-peaked, whereas Schwope et al. (2002) de-

scribes them as being double-peaked. The values of flux and EWs values are found to be variable during the present and previous epochs of observations (see Schwope et al. 2002; Thorstensen et al. 2006, and present work).

3.2. SDSS J075939.79+191417.3

3.2.1. Light Curve Morphology and Power Spectra

Figure 5 shows complete CRTS, R-band, and ZTF-r/g light curves of J0759 where the variable nature of the source is clearly evident. R-band data of the epoch 2021 are found to be observed simultaneously with a few epochs of ZTF in the r and g bands. To probe the system deeply, we have further inspected the temporal properties of J0759 from the CRTS, R-band, and ZTF-r/g band observations separately. We have obtained a total of 17.76 hrs of photometric data from our observations carried over five nights. R-band light curves for five epochs of observations are shown in Figure 6. The light curves of J0759 exhibit a clear eclipse profile with an average dip of ~ 2 mag and eclipse duration of ~ 40 min. Successive eclipses spaced by ~ 3.1 hr were observed on two of the five nights. Similar to the R-band light curve, the ZTF observations of J0759 also reveal the eclipse profiles in their light curves where the brightness drops by ~ 2.0 mag as seen in the R-band light curve. A complete eclipse profile is seen

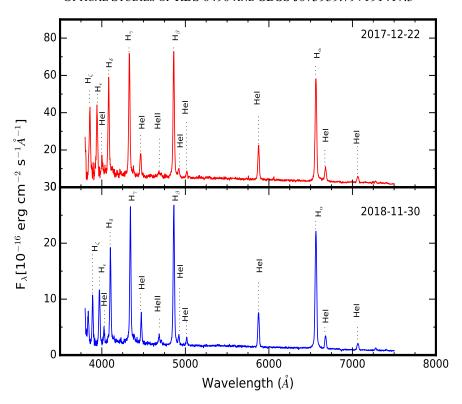


Figure 4. Optical spectra of RBS 0490 for two epochs of observations. The epoch of the observation is mentioned in each panel of the spectrum.

Table 4	Identification	flux FW	and FWHM for	emission fea	tures in the speci	ra of RBS 0490 and J0759.
Table 4.	iuciiuiicauoii.	Hux. E W	allu i willini loi	ciiiissioii ica	itures in the spec	1a 01 KDS 0470 and 10/37.

	RBS 0490												J075	59							
Identification	2017-12-22			2018-11-30		2018-12-17		2019-02-09		2020-01-14		2021-03-31		2021-04-24							
	Flux	-EW	FWHM	Flux	-EW	FWHM	Flux	-EW	FWHM	Flux	-EW	FWHM	Flux	-EW	FWHM	Flux	-EW	FWHM	Flux	-EW	FWHM
Hζ (3889 Å)	126	54	1123	705	108	1535															
$H\epsilon$ (3970 Å)	182	98	1318	696	109	1390															
HeI (4026 Å)	40	18	1094	150	20	1250															
$H\delta$ (4102 Å)	263	93	1132	902	101	1265	41	31	2774	32	36	1926	103	92	3583	50	30	1535	72	39	2304
Hγ (4340 Å)	404	139	1120	1170	141	1217	33	31	2218	34	26	1576	70	51	2142	52	36	1313	50	31	1832
HeI (4471 Å)	84	40	1032	213	33	1125	12	10	2267	3	3	960	26	24	2281	15	14	1140	9	6	1452
CIII/NIII										3	3	918	5	4	776				14	9	2521
(4640/4650 Å)																					
HeII (4686 Å)	27	13	1154	27	4	807	9	7	2286	15	18	960	65	73	1728	38	32	1408	16	11	2091
Hβ (4861 Å)	476	220	1125	1270	188	1111	39	37	1851	35	43	1358	95	84	2036	59	52	1542	57	47	1557
HeI (4922 Å)	28	14	1011	55	8	916				2	3	727	10	9	1286				5	4	1168
HeI (5016 Å)	23	13	970	59	11	978															
HeI (5875 Å)	131	89	1014	3530	70	966	13	19	1736	9	16	1481	28	32	1736	19	23	1021	21	25	1652
$H\alpha$ (6563 Å)	510	341	1024	1280	287	1000	46	94	1582	40	87	1371	78	110	1599	62	81	1188	63	78	1397
HeI (6678 Å)	58	54	1000	136	32	905	9	21	2205	3	8	750	6	37	1438	6	9	898	7	8	1123
HeI (7065 Å)	34	40	1077	81	32	980															

Note—Flux, EW, and FWHM are in the unit of 10^{-16} erg cm⁻² s⁻¹, Å, and km s⁻¹, respectively.

in the ZTF-r band light curve for the epoch 10 December 2019 which is shown in the second panel of Figure 6.

In order to find the periodicity from the eclipsed light curves of J0759, we have performed phase dispersion minimization (PDM; Stellingwerf 1978) algorithm to the combined photometric, ZTF, and CRTS observations. Because of the large data gap between epochs 2016 and 2021, we have used com-

bined photometric data observed during the epoch 2021 for periodogram analysis. The PDM power spectra of R-band, ZTF, and CRTS data are shown in Figure 7. Various prominent peaks are found in the PDM power spectra. The first prominent peak in the PDM periodogram of photometric, ZTF, and CRTS data corresponds to the orbital period of \sim 3.1 hr and perfectly matches with the time-span where pri-

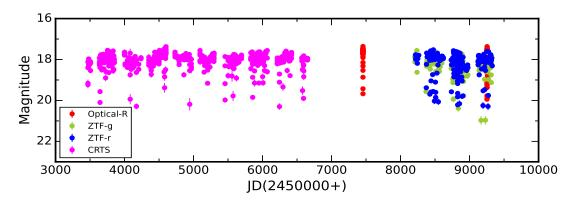


Figure 5. Combined R-band, ZTF-r/g, and CRTS light curve variations of J0759.

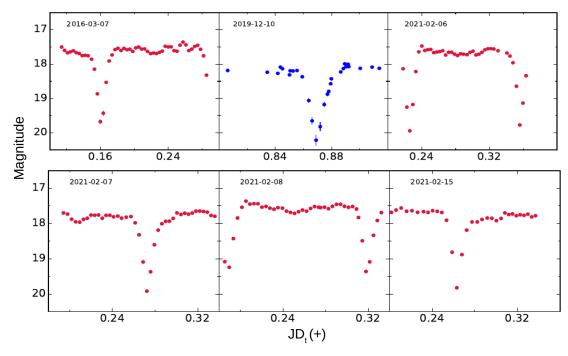


Figure 6. R-band (red) and ZTF-r (blue) light curves of J0759, where the observation day (JD_t) is 2458827.00 for ZTF-r band light curve and for photometric observations it is given in Table 1. The epoch of observations are mentioned at the top of each panel.

mary eclipse completes its one cycle (see Figure 6). Other peaks are also observed in the PDM power spectra which correspond to the harmonics of the orbital frequencies.

ht

3.2.2. Orbital-Phased Light Curve Variations and System's Geometry

We have determined a total of 7 mid-eclipse timings (see Table 5) by fitting a Gaussian function to the bottom part of eclipses. Only those epochs of observations were used for which complete eclipse profiles were observed. A linear least-squares fit to these eclipse timings yields

corresponding to P_{Ω} of 3.14240928±0.00000096 hr. We have also folded the ZTF-r band light curve of the epoch 10 December 2019 and R-band light curves using ephemeris as derived in equation 1. Figure 8 shows the orbital-phase-folded light curves of J0759. Each light curve of J0759 reveals a deep eclipse profile with variable brightness. We have also found evidence of a secondary eclipse near phase 0.5 during all epochs of observations with approximate depths in the range of 0.14-0.3 mag. We could not see any eclipse around phase 0.5 in the ZTF-r band light curve due to its sparse phase coverage.

Using the eclipse width at half depth $(\Delta \phi)$, we derive the orbital inclination of the binary system by using the equation

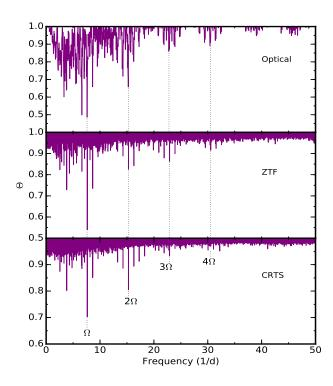


Figure 7. Top to bottom panels show the PDM periodogram of J0759 as obtained from combined R-band photometric, ZTF, and CRTS observations, respectively.

Table 5. Times of minima for J0759 from R-band and ZTF observations.

Date of Obs.	Eclipse Minima (JD)	Cycle
2016 Mar 07	2457455.16058506±0.00014480	0
2019 Dec 10	2458827.86967765±0.00020655	10484.00
2021 Feb 06	2459252.22568635±0.00015772	13725.00
	2459252.35599537±0.00014890	13725.99
2021 Feb 07	2459253.27295816±0.00021381	13732.99
2021 Feb 08	2459254.31926978±0.00025254	13740.99
2021 Feb 15	2459261.26253060±0.00025446	13794.01

given by (Eggleton 1983),

$$\left(\frac{R_2}{a}\right)^2 = \sin^2(\pi\Delta\phi) + \cos^2(\pi\Delta\phi)\cos^2 i,$$
 (2)

where R_2/a depends only on the mass ratio as

$$\frac{R_2}{a} = \frac{Cq^{2/3}}{Dq^{2/3} + \ln(1 + q^{1/3})}. (3)$$

The coefficients C and D are given by Eggleton (1983) as 0.49 and 0.6, respectively for a spherical shape of Roche lobe. However, in the case of CVs, the Roche lobe of secondary is not spherical, having the largest size as "seen" from the white dwarf and the smallest in the polar direction. Therefore, we have used the coefficients C = 0.4990 and D = 0.5053 (Andronov & Andrych 2014). Further, using the same approach as described in section 3.1.2, the mass and radius of the secondary are estimated as $0.28(\pm 0.01) M_{\odot}$ and $0.33(\pm 0.01~R_{\odot})$, respectively. Assuming the minimum and maximum values of WD in CVs of 0.2 M_{\odot} and 1.5 M_{\odot} , the limiting values of q are estimated as 1.4 and 0.19, respectively. For each consecutive epochs of R-band observations (see Table 1) and ZTF-r band observations of the epoch 10 December 2019, the eclipse width at half depth $(\Delta \phi)$ was estimated as 0.081 ± 0.003 , 0.077 ± 0.004 , 0.078 ± 0.005 , 0.082 ± 0.004 , 0.068 ± 0.005 , and 0.087 ± 0.004 , respectively. Adopting the average values of $\Delta \phi$ and q of 0.079±0.002 and 0.35 (assuming the average value of the mass of WD in CVs as $0.8 M_{\odot}$; Zorotovic et al. (2011)), respectively, the orbital inclination (i) is estimated to be $\sim 78^{\circ}$. This estimated value of i is in good agreement with the values derived in terms of the graphical form of the relationship between $\Delta \phi$, i, and q for Roche geometry in Horne (1985). Considering the limiting values of WD masses in CVs, the binary separation is estimated to be in the range of $(5.9-9.2)\times10^{10}$ cm. The mean density of secondary $\overline{\rho}$ is estimated to be 10.8 g cm⁻³, which infers the spectral type and effective temperature of secondary as M4.2 and 3292 K, respectively.

The total duration of an eclipse is approximately 40 min. This measured value of ~ 40 min for the entire eclipse duration is too long to represent an eclipse of just the primary star and can also be used to determine the size of the eclipsed light-producing source. Thus, we have determined the radius of the eclipsed region (R) by using the following equation of Bailey (1990)

$$R = \pi \ a \ \sqrt{(1 - \alpha^2)} \ \Delta \phi_{ie}, \tag{4}$$

where $\Delta\phi_{ie}$ is ingress/egress duration, α = $cos\ i/cos\ i_{lim}$, i is angle of inclination, and i_{lim} is a limiting angle of inclination for which eclipse half-width at half depth reaches zero. The average value of ingress/egress duration ($\Delta\phi_{ie}$) is derived to be 0.14 ± 0.06 , where the error on $\Delta\phi_{ie}$ is the standard deviation of different measurements. Assuming the angle of inclination, $i \sim 78^\circ$, average value of q=0.35, and using i_{lim} from the Table 1 of Bailey (1990), the value of R is estimated to be $\sim 33\ R_{WD}$, where R_{WD} is calculated using the mass-radius relation given by Nauenberg (1972).

3.2.3. Optical Spectroscopy

Optical spectra of J0759 obtained for five epochs of observations are shown in Figure 9. The orbital phase for every epoch of observations was derived using mid-time of expo-

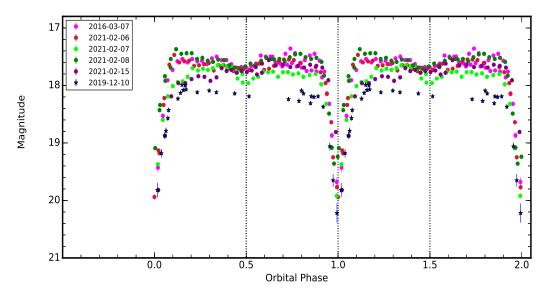


Figure 8. Orbital-phase-folded light curves of J0759 in R-and ZTF-r bands.

sure and the equation 1. In each spectrum, we have observed strong Balmer emission lines from H\$\alpha\$ to H\$\delta\$, along with the He I and weak He II (\$\lambda 4686 \delta\$) lines. We have also found the weak Bowen fluorescence CIII/NIII emission lines in the spectra of J0759. These emission lines are found to be variable from one epoch of observation to another. The current optical spectra of J0759 resemble the earlier observed optical spectrum from the SDSS as obtained by Szkody et al. (2006) during the epoch 06 November 2004. The SDSS flux of the emission lines H\$\alpha\$, H\$\beta\$, and He I (\$\lambda\$ 4471 \delta\$) seems to be consistent with the observed flux for the epoch 09 February 2019, however, the strength of emission line He II (\$\lambda\$4686 \delta\$) was relatively weak in the SDSS spectrum (Szkody et al. 2006).

4. DISCUSSION

We have carried out detailed analyses of two CVs – RBS 0490 and J0759, using optical photometry and spectroscopy. We discover a photometric period of 1.689±0.001 hr for RBS 0490, which is probably its orbital period. For J0759, our eclipse timings confirm and refine the previously determined period of 3.14-hr. The orbital period of RBS 0490 and J0759 place them below and above the period gap of orbital period distribution of CVs, respectively.

The absolute value of G-band magnitude is approximately +9.9 mag for RBS 0490 which appears to be similar to that for the magnetic systems of AM Her types. Further, the photometric light curve variations in RBS 0490 also look similar to a magnetic system, possibly polars, and these variations are unusual for an ordinary nova-like or a dwarf nova. These light curve variations reveal interesting one broad hump and then a second hump or a plateau-like structure. The main

broad hump can be associated with the main accretion region. However, the observed second hump or plateau-like structure indicates that the minimum might be filled up by the emission of an independent second accretion region or may indicate accretion at a second fainter pole. The accretion onto a second pole has been seen in a few polars, e.g. in DP Leo (Cropper 1990), VV Pup (Wickramasinghe et al. 1989), UZ For (Schwope et al. 1990), and QS Tel (Schwope et al. 1995), etc. In the majority of the cases, the activity from the second pole is at least one order of magnitude lower as compared to the primary one. The polarimetric observations of RBS 0490 can help to confirm the two-pole accretion in the future.

R-band light curves of J0759 exhibit deep eclipses with an average magnitude of the depth of ~ 2.0 mag. The observed eclipse resembles the disc rather than the highly structured eclipses often seen in AM Her stars. The absolute G-band magnitude implied by the Gaia parallax is near +6.5, significantly brighter than most magnetic systems. Further, the large value of eclipse radius indicates that the eclipse observed in the light curves is not solely due to the occultation of WD by secondary. In general, the dimension of the optical emission sites is thought to be < 0.1 R_{WD} (Bailey & Cropper 1991). Therefore, the derived large value of R indicates that the eclipse feature might be observed due to the occultation of the accretion disc and bright spot.

The optical spectra of J0759 show strong Balmer emission lines, He I, and He II along with conspicuous features of weak He II (λ 4686 Å) and Bowen fluorescence CIII/NIII emission lines. The weakness of HeII λ 4686 and the Bowen lines suggest that J0759 is not a magnetic CV (Warner 1995). However, this is not a sufficient criterion for a CV classification. More specifically, the ratio of EW[He II (λ 4686)/ $H\beta$]

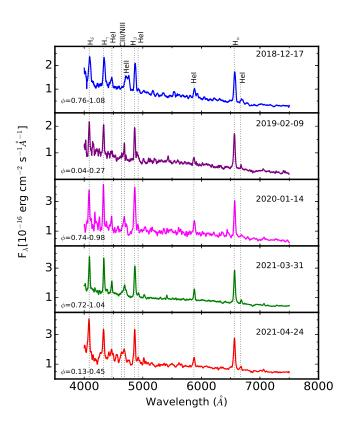


Figure 9. Optical spectra of J0759 for five epochs of observations. The date of observation and corresponding orbital phase are mentioned in each panel of the spectrum.

and EW of $H\beta$ emission line provides a criterion to separate magnetic CVs from non-magnetic CVs (Silber et al. 1992). According to Silber's criteria - magnetic CVs are characterized by the ratio EW[He II $(\lambda 4686)/H\beta$] ≥ 0.4 and $H\beta \geq$ 20 Å. For J0759, we have detected the $H\beta \ge 20$ Å for all observations, however, the EW ratio of He II (λ 4686) to $H\beta$ is not detected more than 0.4 for all epochs of observations. For the epochs 17 December 2018 and 24 April 2021, we have observed this ratio is close to 0.2, which is not quite up to the values for magnetic CVs. The Balmer decrement can also be used in order to distinguish the magnetic and non-magnetic nature of the system. The inverted Balmer decrement is possibly present in the low-state spectra of the AM Her type of magnetic CVs. However, a flat Balmer decrement, implying that the Balmer emission lines are optically thick, has been observed in most of the non-magnetic CVs and also in intermediate polars (Warner 1995). For J0759, a flat Balmer decrement is observed in the most epoch of observations. The cyclotron hump features are also not detected in the optical spectra of J0759. Thus, it appears that the system J0759 follows the majority of the criteria of being non-magnetic but further observations are needed for definitive classification.

In the case of RBS 0490, optical spectra also consist of strong emission lines of Balmer series and He I together

with the weak emission line of He II (λ 4686). The presence of single-peaked strong Balmer emission lines and the large equivalent width of the H β emission line may imply a magnetic CV classification for this system. However, other possible factors like weak He II (λ 4686 Å), broad Balmer emission lines, the observed flat Balmer decrement, the ratio of EW[He II (λ 4686)/H β] ~ 0.1 and 0.02 (for epochs 22 December 2017 and 30 November 2018), and the non-detection of cyclotron hump in the optical spectrum either weakens its chance to be magnetic or may imply the low magnetic strength of the WD. A low magnetic field strength of the WD was also proposed by Harrison & Campbell (2015) from the combined WISE and JHK observations of RBS 0490.

5. CONCLUSIONS

We have presented the optical photometric and spectroscopic observations of RBS 0490 and J0759 which leads us to the following conclusions:

 RBS 0490 has been found to vary with a period of 1.689±0.001 hr, which was not evident in earlier studies and can be interpreted as its orbital period. The probable orbital period places it below the period gap of the orbital period distribution of CVs. The variability observed in RBS 0490 seems to favour the magnetic

systems, possibly polars, and provide evidence of the emission from an independent second accretion region or a second fainter pole. However, the characteristic features seen in the optical spectra of RBS 0490 either weaken its chance to be magnetic or may imply the low magnetic strength of the WD.

Our eclipse photometry confirms and refines the ~ 3.14 hr period of J0759, placing it longward of the period gap. The eclipses are consistent with a disc and an orbital inclination of ~ 78°. The detection of strong Balmer emission lines along with the weak high ionization emission lines hint towards the non-magnetic nature of J0759.

ACKNOWLEDGEMENTS

We acknowledge the referee for useful comments and suggestions that improved the manuscript considerably. This work is supported by the National Key Research and Development Program of China (Grants No. 2021YFA0718500, 2021YFA0718503), the NSFC (12133007, U1838103, 11622326), and the Fundamental Research Funds for the Central Universities (No. 2042021kf0224). This research includes data collected with the TESS mission, obtained from the MAST data archive at the Space Telescope Science In-

stitute (STScI). Funding for the TESS mission is provided by the NASA Explorer Program. STScI is operated by the Association of Universities for Research in Astronomy, Inc., under NASA contract NAS 5-26555. Based on observations obtained with the Samuel Oschin 48-inch and the 60-inch Telescope at the Palomar Observatory as part of the Zwicky Transient Facility project. ZTF is supported by the National Science Foundation under Grant No. AST-1440341 and AST-2034437 and a collaboration including Caltech, IPAC, the Weizmann Institute for Science, the Oskar Klein Center at Stockholm University, the University of Maryland, the University of Washington, Deutsches Elektronen-Synchrotron and Humboldt University, Los Alamos National Laboratories, the TANGO Consortium of Taiwan, the University of Wisconsin at Milwaukee, Trinity College Dublin, Lawrence Livermore National Laboratories, Lawrence Berkeley National Laboratories, and IN2P3, France. Operations are conducted by COO, IPAC, and UW. One of the authors Ashish Raj acknowledges the Research Associate Fellowship with order no. 03(1428)/18/EMR-II under Council of Scientific and Industrial Research (CSIR). The observing staff and observing assistants of 1-m and 2-m class telescopes are deeply acknowledged for their support during optical observations.

REFERENCES

Andronov, I. L., & Andrych, K. D. 2014, Odessa Astronomical Publications, 27, 38. https://arxiv.org/abs/1411.3884

Bailey, J. 1990, MNRAS, 243, 57, doi: 10.1093/mnras/243.1.57

Bailey, J., & Cropper, M. 1991, MNRAS, 253, 27,

doi: 10.1093/mnras/253.1.27

Beardmore, A. P., Ramsay, G., Osborne, J. P., et al. 1995, MNRAS, 273, 742, doi: 10.1093/mnras/273.3.742

Bellm, E., Kulkarni, S., & Graham, M. 2019, in AmericanAstronomical Society Meeting Abstracts, Vol. 233, AmericanAstronomical Society Meeting Abstracts #233, 363.08

Beuermann, K., Baraffe, I., Kolb, U., & Weichhold, M. 1998, A&A, 339, 518

Bridge, C. M., Cropper, M., Ramsay, G., et al. 2003, MNRAS, 341, 863, doi: 10.1046/j.1365-8711.2003.06456.x

Cropper, M. 1990, SSRv, 54, 195, doi: 10.1007/BF00177799

Dekany, R., Smith, R. M., Riddle, R., et al. 2020, PASP, 132, 038001, doi: 10.1088/1538-3873/ab4ca2

Drake, A. J., Djorgovski, S. G., Mahabal, A., et al. 2009, ApJ, 696, 870, doi: 10.1088/0004-637X/696/1/870

Drake, A. J., Gänsicke, B. T., Djorgovski, S. G., et al. 2014, MNRAS, 441, 1186, doi: 10.1093/mnras/stu639

Eggleton, P. P. 1983, ApJ, 268, 368, doi: 10.1086/160960

Gaia Collaboration, Brown, A. G. A., Vallenari, A., et al. 2021, A&A, 650, C3, doi: 10.1051/0004-6361/202039657e

Gänsicke, B. T., & Dillon, M. 2009, MNRAS, 397, 2170, doi: 10.1111/j.1365-2966.2009.15126.x

Graham, M. J., Kulkarni, S. R., Bellm, E. C., et al. 2019, PASP, 131, 078001, doi: 10.1088/1538-3873/ab006c

Harrison, T. E., & Campbell, R. K. 2015, ApJS, 219, 32, doi: 10.1088/0067-0049/219/2/32

Horne, J. H., & Baliunas, S. L. 1986, ApJ, 302, 757, doi: 10.1086/164037

Horne, K. 1985, MNRAS, 213, 129, doi: 10.1093/mnras/213.2.129

Knigge, C. 2006, MNRAS, 373, 484,

doi: 10.1111/j.1365-2966.2006.11096.x

Lomb, N. R. 1976, Ap&SS, 39, 447, doi: 10.1007/BF00648343

Mason, P. A., Ramsay, G., Andronov, I., et al. 1998, MNRAS, 295, 511, doi: 10.1046/j.1365-8711.1998.01185.x

Nauenberg, M. 1972, ApJ, 175, 417, doi: 10.1086/151568

Patterson, J. 1994, PASP, 106, 209, doi: 10.1086/133375

Prabhu, T. P., & Anupama, G. C. 2010, in Astronomical Society of India Conference Series, Vol. 1, Astronomical Society of India Conference Series

- Ricker, G. R., Winn, J. N., Vanderspek, R., et al. 2015, Journal of Astronomical Telescopes, Instruments, and Systems, 1, 014003, doi: 10.1117/1.JATIS.1.1.014003
- Rosen, S. R., Mittaz, J. P. D., Buckley, D. A., et al. 1996, MNRAS, 280, 1121, doi: 10.1093/mnras/280.4.1121
- Sagar, R., Omar, A., Kumar, B., et al. 2011, Current Science, 101, 1020
- Salvi, N., Ramsay, G., Cropper, M., Buckley, D. A. H., & Stobie, R. S. 2002, MNRAS, 331, 488,
 - doi: 10.1046/j.1365-8711.2002.05216.x
- Scargle, J. D. 1982, ApJ, 263, 835, doi: 10.1086/160554
- Scaringi, S., Bird, A. J., Norton, A. J., et al. 2010, MNRAS, 401, 2207, doi: 10.1111/j.1365-2966.2009.15826.x
- Schmidt, G. D., Hoard, D. W., Szkody, P., et al. 1999, ApJ, 525, 407, doi: 10.1086/307901
- Schwope, A. D., Beuermann, K., & Thomas, H.-C. 1990, A&A, 230, 120
- Schwope, A. D., Brunner, H., Buckley, D., et al. 2002, A&A, 396, 895, doi: 10.1051/0004-6361:20021386
- Schwope, A. D., Thomas, H. C., & Beuermann, K. 1993, A&A, 271, L25
- Schwope, A. D., Thomas, H. C., Beuermann, K., et al. 1995, A&A, 293, 764

- Silber, A., Bradt, H. V., Ishida, M., Ohashi, T., & Remillard, R. A. 1992, ApJ, 389, 704, doi: 10.1086/171243
- Sinvhal, S. D., Kandpal, C. D., Mahra, H. S., Joshi, S. C., & Srivastava, J. B. 1972, in Optical astronomy with moderate size telescopes, Symposium held at Centre of Advanced STudy in Astronomy, Osmania Univ., Hyderabad, p. 20 34 = Uttar Pradesh State Obs., Naini Tal, Repr. No. 64, Vol. 64, 20–34
- Smith, D. A., & Dhillon, V. S. 1998, MNRAS, 301, 767, doi: 10.1046/j.1365-8711.1998.02065.x
- Stellingwerf, R. F. 1978, ApJ, 224, 953, doi: 10.1086/156444Szkody, P., Henden, A., Agüeros, M., et al. 2006, AJ, 131, 973, doi: 10.1086/499308
- Thorstensen, J. R., Lépine, S., & Shara, M. 2006, PASP, 118, 1238, doi: 10.1086/507956
- Voges, W., Aschenbach, B., Boller, T., et al. 1999, A&A, 349, 389Warner, B. 1986, MNRAS, 219, 347, doi: 10.1093/mnras/219.2.347
- —. 1995, Cambridge Astrophysics Series, 28
- Wickramasinghe, D. T., Ferrario, L., & Bailey, J. 1989, ApJL, 342, L35, doi: 10.1086/185478
- Zorotovic, M., Schreiber, M. R., & Gänsicke, B. T. 2011, A&A, 536, A42, doi: 10.1051/0004-6361/201116626